ELECTRONIC SUPPLEMENTARY INFORMATION

Ultrafast flavin photoreduction in an oxidized animal (6-4) photolyase through an unconventional tryptophan tetrad

Ryan Martin,[a,b] Fabien Lacombat,[a,b] Agathe Espagne,[a,b] Nadia Dozova,[a,b] Pascal Plaza*,[a,b] Junpei Yamamoto,[c] Pavel Müller,[d] Klaus Brettel[d] and Aurélien de la Lande[e]

[a] *PASTEUR, Département de chimie, École normale supérieure, UPMC Univ. Paris 06, CNRS, PSL Research University, 75005 Paris, France*
[b] *Sorbonne Universités, UPMC Univ. Paris 06, École normale supérieure, CNRS, PASTEUR, 75005 Paris, France*
[c] *Division of Chemistry, Graduate School of Engineering Science, Osaka University, 1-3 Machikaneyama, Toyonaka, Osaka 560-8531, Japan*
[d] *Institute for Integrative Biology of the Cell (I2BC), Joliot, CEA, CNRS, Univ. Paris-Sud, Université Paris-Saclay, 91198 Gif-sur-Yvette cedex, France*
[e] *Laboratoire de Chimie Physique, CNRS, Université Paris-Sud, Université Paris Saclay, Orsay F-91405, France*

Contents

1. Homology modeling 2
2. Molecular dynamics 3
3. Theoretical anisotropies 4
4. Analysis of the steady-state absorption spectra 6
5. Polarized transient absorption spectra 8
6. Global analysis of the polarized transient absorption data 9
7. Reference absorption spectra used for the identification of the photoproducts 13
8. Quantum yield of charge separation 14
9. Nanosecond anisotropy measurements 16
10. Basic reaction scheme 17

1. Homology modeling

In order to construct a homology model of the *Xenopus laevis* (6-4) photolyase (Xl64), it was first necessary to perform a sequence alignment with the structure to be used as a template, that is, *Drosophila melanogaster* (6-4) photolyase (Dm64; PDB: 3CVU[1]). This was done with ClustalW2.[†] The two proteins share 57% identity and 78% similarity. The alignment was in fact made for various members of the cryptochrome/photolyase family and Table S1 shows the result in the region containing the Trp tetrad.

Table S1. Sequence alignment of several members of the cryptochrome/photolyase family. CPD in the protein name stands for CPD photolyase, 64 for (6-4) photolyase and Cry for cryptochrome. The tryptophans discussed in the text have been highlighted and labeled.

The proteins come from the following organisms: *Escherichia coli* (Ec), *Thermus thermophilus* (Tt), *Anacystis nidulans* (An), *Dunaliella salina* (Ds), *Arabidopsis thaliana* (At), *Drosophila melanogaster* (Dm), *Danio rerio* (Dr), *Xenopus laevis* (Xl), *Ostereococcus tauri* (Ot), *Phaeodactylum tricornutum* (Pt), *Erithacus rubecula* (Er), *Gallus gallus* (Gg), *Mus musculus* (Mm), and *Homo sapiens* (Hs).

The sample sequences were obtained from NCBI, with the accession numbers of P00914.1, BAA22943.1, P05327.4, AAX56342.1, BAA24449.1, AAN11080.1, BAA96852.1, BAA97126.1, NP_567341.1, NP_849588.1, Q84KJ5.2, CEF96928.1, EEC48286.1, O77059.1, BAA96846.1, BAA96848.1, BAA96851.1, NP_001088990.1, NP_001083936.1, NP_001084438.1, AAW48290.1, NP_989576.1, NP_989575.1, NP_001034685.1, NP_031797.1, NP_034093.1, NP_004066.1 and NP_066940.2, in order of the list.

		W_C	$W_{B'}$	W_D W_B	W_A $W_{A'}$	
EcCPD	295	HRPFIAWTDR	VQWQSN-PAH	LQAWQEGKTG	YPIVDAAMRQ	392
TtCPD	263	ERPLDPRFQA	LPWQED-EAL	FRAWYEGRTG	VPLVDAAMRE	360
AnCPD	302	DGPYRSLWQQ	FPWENR-EAL	FTAWTQAQTG	YPIVDAAMRQ	399
Ds64	354	RIAGNPICRQ	ITWDTN-PAL	LKAWRDGATG	YPWIDAAMTQ	452
At64	317	KMKGNRICKQ	IPWNED-HAM	LAAWRDGKTG	YPWIDAIMVQ	415
Dm64	318	RMLGNVYCMQ	IPWQEH-PDH	LEAWTHGRTG	YPFIDAIMRQ	416
Dr64	307	KMEGNSACVQ	VDWDNN-PEH	LAAWREARTG	FPFIDTIMTQ	405
Xl64	307	KMEGNPVCVQ	VDWDNN-KEH	LEAWSEGRTG	YPFIDAIMTQ	405
AtCry1	312	ERPLLGHLKF	FPWAVD-ENY	FKAWRQGRTG	YPLVDAGMRE	409
AtCry2	307	EQSLLSHLRF	FPWDAD-VDK	FKAWRQGRTG	YPLVDAGMRE	406
AtCry3	388	FHLGGPRNVQ	GKWSQD-QKL	FESWRDAKTG	YPLIDANMKE	485
OtCPF1	339	FHLDGTAGRR	ASWKRD-EKI	LKAWKTGTTG	YPLIDANMRE	436
PtCPF1	339	KMIDNPIARQ	IPWDDD-PDL	LLAWKMSKTG	YPYIDAIMTQ	437
DmCry1	330	RMEGNDICLS	IPWAKPNENL	LQSWRLGQTG	FPLIDGAMRQ	429
DrCry1a	308	KMEGNPICVQ	IPWDKN-PEA	LAKWAEGRTG	FPWIDAIMTQ	406
DrCry2a	308	KMEGNPICVR	IPWDKN-PEA	LAKWAEAKTG	FPWIDAIMTQ	406
DrCry4	305	KMEGNSICLQ	IDWYHD-PER	LEKWRTAQTG	FPWIDAIMTQ	403
XlCry1	307	HMVGNPICLQ	IPWYKN-EEQ	LQKWREGKTG	FPWIDAIMAQ	405
XlCry2	312	QMEGNPICVQ	IPWDKN-PKA	LAKWTEGKTG	FPWIDAIMTQ	410
XlCryD	312	FFLRGLQDKD	IPWKRD-PKL	FDAWKEGRTG	VPFVDANMRE	409
ErCry1a	308	KMEGNPICVQ	IPWDKN-PEA	LAKWAEGRTG	FPWIDAIMTQ	406
GgCry1	308	KMEGNPICVQ	IPWDKN-PEA	LAKWAEGRTG	FPWIDAIMTQ	406
GgCry2	317	RMEGNPICIQ	IPWDKN-PEA	LAKWAEGKTG	FPWIDAIMTQ	415
GgCry4	306	KMAGNPICLQ	IRWYED-AER	LHKWKTAQTG	FPWIDAIMTQ	404
MmCry1	308	KMEGNPICVQ	IPWDKN-PEA	LAKWAEGRTG	FPWIDAIMTQ	406
MmCry2	326	RMEGNPICIQ	IPWDRN-PEA	LAKWAEGKTG	FPWIDAIMTQ	424
HsCry1	318	KMEGNPICVQ	IPWDKN-PEA	LAKWAEGRTG	FPWIDAIMTQ	416
HsCry2	348	RMEGNPICIQ	IPWDRN-PEA	LAKWAEGKTG	FPWIDAIMTQ	446

The model was created using the online SWISS-MODEL platform.[‡2] In brief, the method consists in threading the target sequence around the structure of the template and then optimizing

[†] http://www.ebi.ac.uk/Tools/msa/clustalw2/

[‡] http://swissmodel.expasy.org/

the orientation of the residues to match the crystal structures of other similar proteins. The flavin cofactor is inserted thereafter, as in the template.

2. Molecular dynamics

The structure constructed by homology modeling was relaxed by a long MD simulation of 125 ns. We used the standard Amberff99 force field and the NAMD program.[3] The parameters for the oxidized FAD cofactor was taken from Cailliez *et al*.[4] The protein was solvated in a water box of TIP3P molecules of dimension 113×108×100 $Å^3$. Electrostatic interactions were computed using the Particle Mesh Ewald summation. We used a cutoff of 9 Å, using a switching function to truncate Lennard-Jones and electrostatic potentials are truncated. The Shake algorithm was used to constrain bonds including hydrogen atoms and a time step of 1 fs is used. Simulations were performed in the isothermal-isobaric NPT ensemble at 300 K and under a pressure of 1 atmosphere. Temperature was controlled by applying Langevin forces with a damping coefficient of 1 ps^{-1}. The pressure was controlled using a Nosé-Hoover Langevin piston. After 10000 steps of geometry optimization the system was gradually heated from 25 to 300 K with harmonic restraints (50 kcal/mol/$Å^2$) imposed on protein heavy atom positions. At each temperature the system was relaxed for 500ps. The heating phase was followed by 4×500 ps MD simulations in the NPT ensemble in which the restraints on the positions of heavy atoms were progressively released by setting the constraining force constant to 20, 10, 5 and finally 1 kcal/mol/$Å^2$. NPT simulations were then conducted for 125 ns with the NAMD program. The Root-Mean-Square Deviation on the protein atoms is shown on Fig. S1, attesting the overall stability of the homology modeled structure. A thorough analysis of the tryptophan tetrad residues and of the FAD cofactor showed that no significant modifications of the relative orientations of these molecular fragments took place during the 125-ns MD simulations. We created an average structure taking the last 25 ns of the simulation to determine a reference structure for the analysis of the experimental anisotropy (see below).

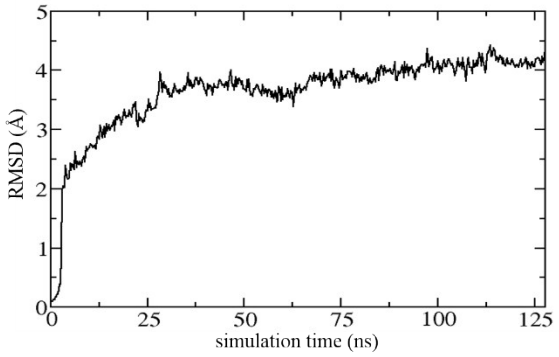

Fig. S1. Root-Mean-Square-Deviation of Xl(6-4) PL protein atoms along 125 ns of classical MD simulations.

3. Theoretical anisotropies

3.1 Probing the orientation of the tryptophanyl radicals

Let us first recall that, to probe the orientation of the $WH^{\bullet+}$ radicals with the anisotropy tool, it is highly preferable to choose conditions where a single transition is excited and a single transition is probed. In that case, the anisotropy simply depends on the angle (β) between the transition dipole moment of the excitation transition and the transition dipole moment of the probed transition,[5,6] as given by Equation S1.

$$r = (3\,cos^2\beta - 1)/5 \qquad \text{(S1)}$$

In our transient absorption experiments, the pump beam at 475 nm solely excites the $S_0 \rightarrow S_1$ transition of the flavin, which satisfies the first condition. Fig. S11 below (§7) shows that the spectral region around 615 nm is well suited for the second condition. The reference absorption spectrum of $WH^{\bullet+}$ has a red-most maximum at *ca.* 590 nm, which can be recognized around 615 nm in Xl64. At this wavelength, the contributions of FAD_{ox} and $FAD^{\bullet-}$ can be neglected.

3.2 Direction of the transition dipole moments

In order to calculate the angle β using our homology model, it is first necessary to define the directions of the relevant transition dipole moments within the molecular frameworks of the FAD_{ox} and $WH^{\bullet+}$ species.

Some values may be found in the literature. Using the polarized absorption of a single crystal of oxidized flavodoxin, Eaton *et al.*[7] reported the angle between the transition moment and the

short axis of the molecule to be 75° ± 4° (counted counterclockwise; see Fig. S2-A). This value is supported by the computational study of Climent *et al.*[8] Byrdin *et al.*[5§] reported that the transition dipole moment of $WH^{\bullet+}$ makes an angle of 110°, counted counterclockwise, with respect to the short axis of the molecule (see Fig. S2-B).

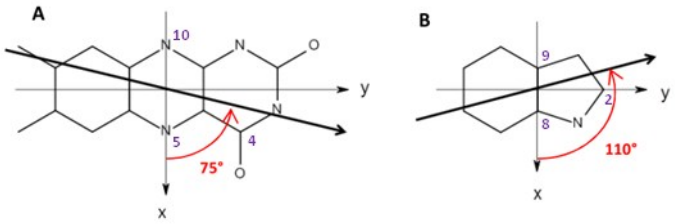

Fig. S2. A) Orientation of the transition dipole moment for the lowest transition of the isoalloxazine ring of FAD (75° counted counterclockwise from x axis), according to Eaton *et al.*[7] B) Orientation of the transition dipole moment for the lowest transition of the indole ring of the $WH^{\bullet+}$ radical (110° from x axis), according to Crespo *et al*.[9]

For the present work, we carried out Time-Dependent Density Functional Theory calculation along our previously reported MD simulation of the protein.[4] 50 snapshots were extracted from these simulations and we computed the transition dipole moments by a QM/MM approach. Either the flavin or the tryptophan was included in the QM partition. We used the ωB97XD exchange-correlation functional[10] coupled to the 6-311G** basis set. These calculations yielded average values of 73° for FAD_{ox} and 107.7° for $WH^{\bullet+}$ (same conventions as above), which are essentially identical to the values of the literature, to within a couple of degrees. These values were used to produce the predictions of anisotropy presented below.

The molecular plane, and attached x and y axes, were defined for each molecule with the help of three atoms: N10, N5 (defining x) and C4 (defining y, orthogonally to x) for FAD_{ox} (see Fig. S2-A) and C9, C8 (x) and C2 (y) for $WH^{\bullet+}$ (Fig. S2-B).

3.3 Predictions of intrinsic anisotropies

The predictions of intrinsic anisotropies associated to each relevant Trp of the photoreduction site were done in two ways: using our homology model (HM) of Xl64, on the one hand, and using the average structure derived from our MD simulation (§2), on the other hand.

§ This information, deriving from DFT calculations, comes in fact from a personal communication with D.A. Estrin, corresponding author of Crespo *et al*.[7]

Table S2 lists the various β angles, together with a rough estimation of the corresponding errors. To calculate the errors, the intrinsic orientations of both transition moments in the molecular frame of reference were allowed to vary within an interval of ± 4° within the plane of the molecules. This choice hopefully gives an upper value of the degree uncertainty attached to β, taking into account the various values for the directions of the relevant transition dipole moments available to us (literature and present work) and, to a lesser extent, the precise definition of the x and y axes (see above).

Table S2. Angle β (expressed in degrees) associated to the different $WH^{\bullet+}$ radicals present in the photoreduction site, according to the homology model (HM) or the MD simulation.

	W_A	W_B	W_C	W_D	$W_{A'}$	$W_{B'}$
HM	53.5° ± 5.3°	150.8° ± 4.3°	62.3° ± 6.6°	75.3° ± 3.4°	89.2° ± 6.6°	147.3° ± 5.5°
MD	47.0° ± 5.6°	139.7° ± 3.9°	64.4° ± 6.4°	70.8° ± 3.0°	100.1° ± 3.6°	129.6° ± 3.8°

Theoretical anisotropies (and corresponding errors) were then deduced from β with Equation S1 and are listed in Table S3.

Table S3. Intrinsic anisotropies associated to the different $WH^{\bullet+}$ radicals present in the photoreduction site, according to the homology model (HM) or the MD simulation.

	W_A	W_B	W_C	W_D	$W_{A'}$	$W_{B'}$
HM	0.012 ± 0.053	0.257 ± 0.038	-0.070 ± 0.057	-0.161 ± 0.017	-0.200 ± 0.002	0.225 ± 0.053
MD	0.079 ± 0.058	0.149 ± 0.041	-0.088 ± 0.053	-0.135 ± 0.019	-0.181 ± 0.013	0.044 ± 0.039

4. Analysis of the steady-state absorption spectra

In order to determine the composition of our Xl64 samples (in 50 mM Tris buffer solution at pH 8, with 50 mM NaCl and 20% (v/v) glycerol), we performed a fit of their absorption spectra by a weighted sum of reference spectra of the FAD_{ox}, $FADH^{\bullet}$ and $FADH^{-}$ species, bound to Xl64, as available in the literature. The spectra of FAD_{ox} and $FADH^{\bullet}$ were taken from Schleicher *et al.*[11] (reproduced in Fig. S3-C; see also Müller *et al.*[12]); the spectrum of $FADH^{-}$ comes from Yamamoto *et al.*[13] (Fig. S3-C).

The fit is excellent for WT-Xl64 (Fig. S3-A) and indicates that FAD_{ox} is by far the most abundant species, with a fitted concentration of 178 ± 0.3 µM. The concentrations of $FADH^{\bullet}$ and $FADH^{-}$ are very small: 0.003 ± 0.5 µM and 0.4 ± 0.6 µM, respectively. Given these latter errors exceed the fitted value, it may be concluded that the relative concentrations of $FADH^{\bullet}$ and $FADH^{-}$ are less than 0.3% and 0.6%, respectively. The fit is somewhat poorer for W370F-Xl64, yielding however still a dominant contribution of FAD_{ox} (250 ± 2 µM), with less than 1.2% of each $FADH^{\bullet}$ and $FADH^{-}$.

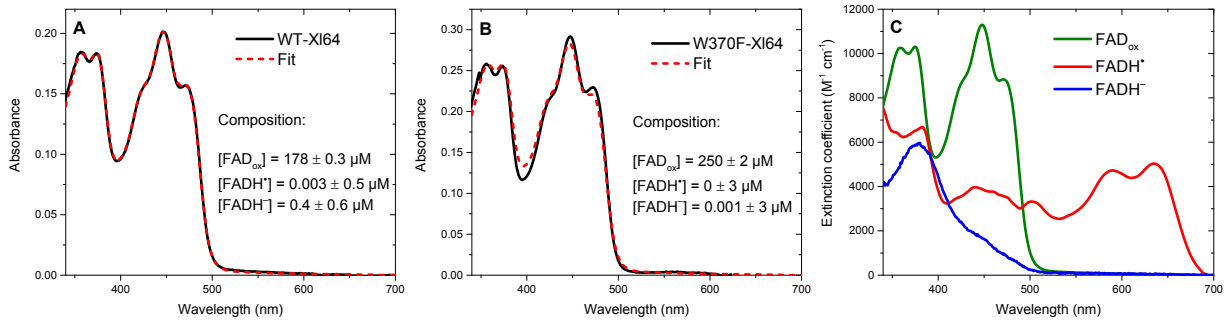

Fig. S3. A) Absorption spectrum of the WT-Xl64 sample (black line) in 50 mM Tris buffer solution at pH 8, with 50 mM NaCl and 20% (v/v) glycerol. The spectral fit is represented in red dotted line. B) Absorption spectrum of W370F-Xl64 and its fit. C) Reference spectra (see text).

5. Polarized transient absorption spectra

The transient absorption spectra of Xl64 were recorded in both parallel and perpendicular polarizations. Fig. S4 presents them for WT and Fig. S5 for W370F.

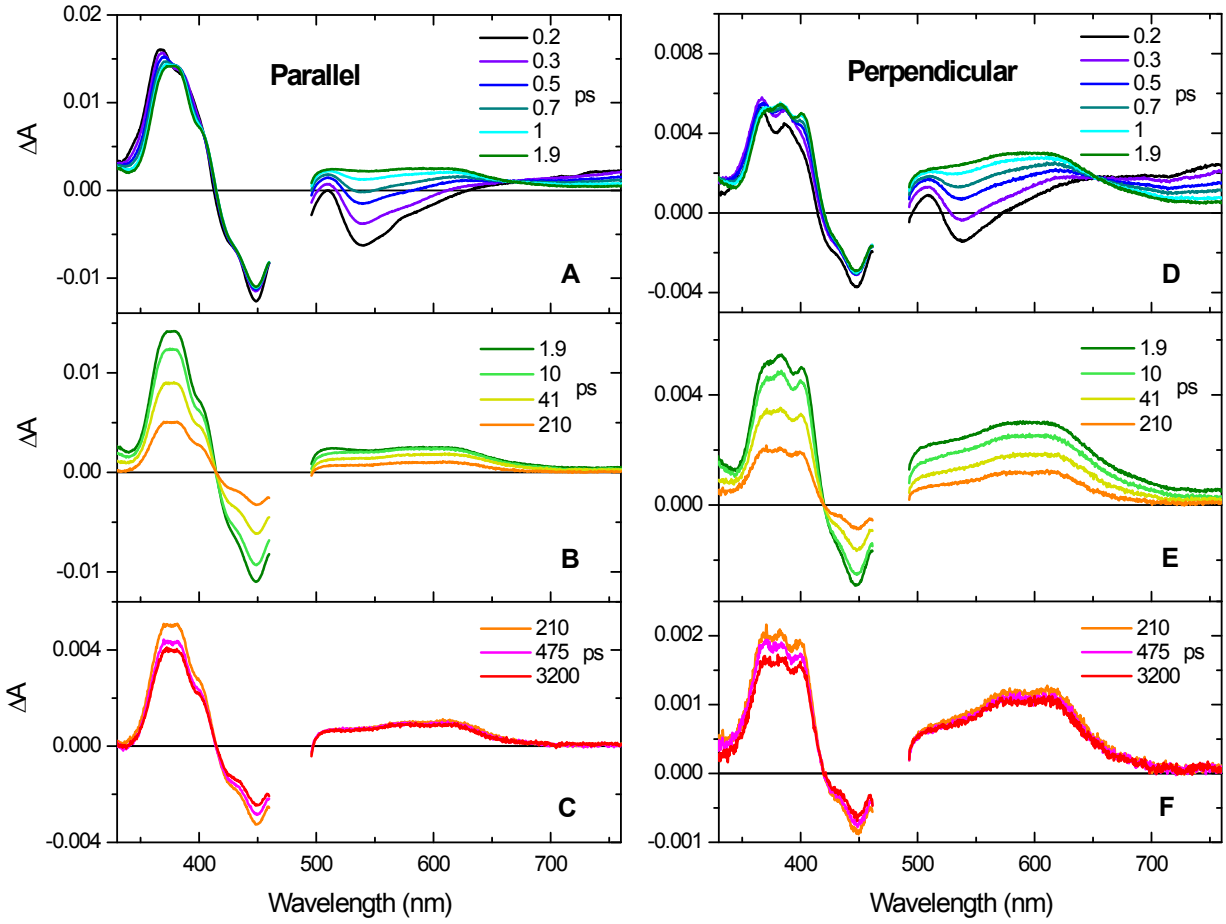

Fig. S4. Polarized transient absorption spectra of WT-Xl64 at different pump-probe delays, indicated in ps in the legends. Panels A to C correspond to the parallel polarization and panels D to F to the perpendicular polarization.

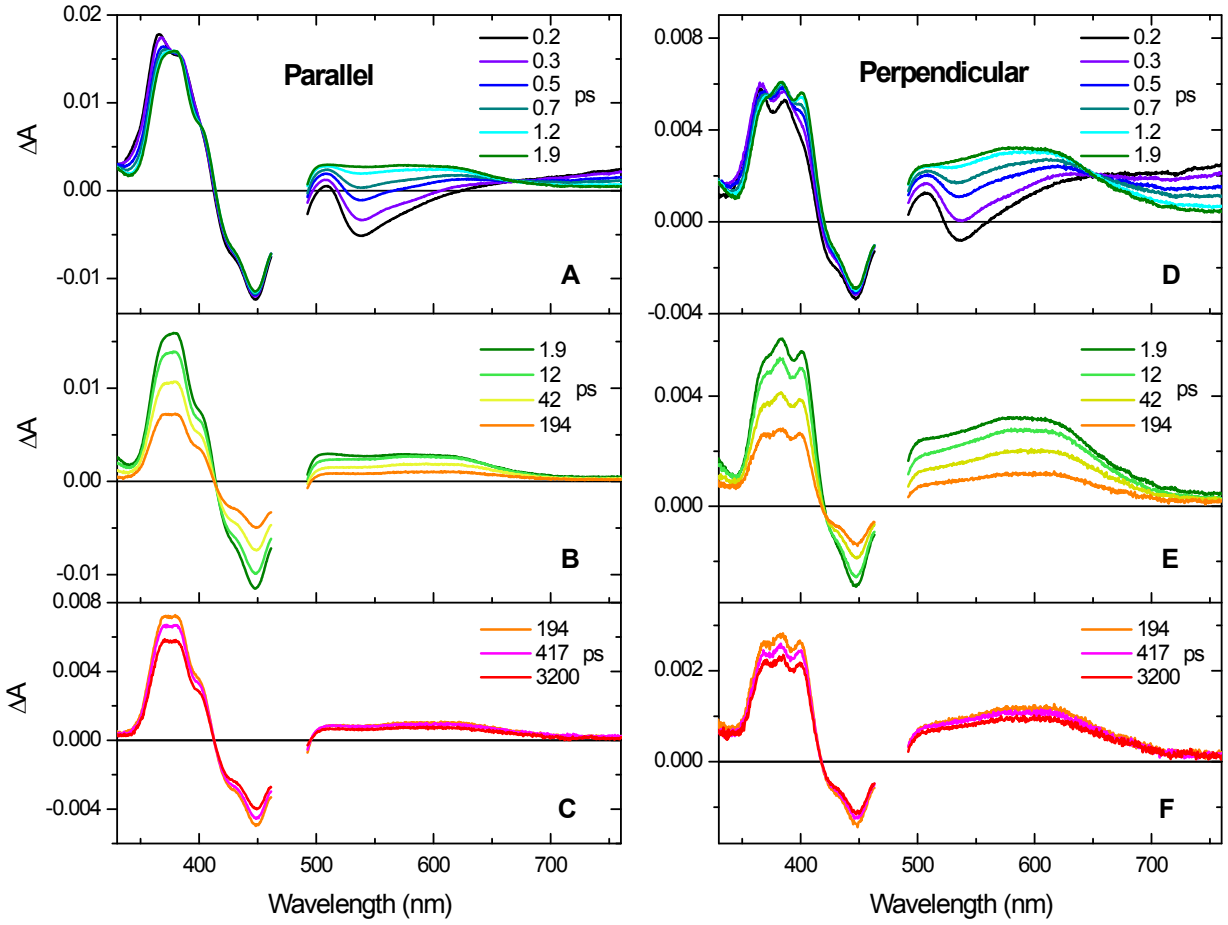

Fig. S5. Polarized transient absorption spectra of W370F-Xl64 at different pump-probe delays, indicated in ps in the legends. Panels A to C correspond to the parallel polarization and panels D to F to the perpendicular polarization.

6. Global analysis of the polarized transient absorption data

The parallel and perpendicular transient absorption spectra of Xl64 were simultaneously and globally fitted with a sum of 4 exponential components followed by a plateau. Table S4 gathers the obtained time constants for both WT and W370F. Very similar time constants were obtained upon global fitting of the isotropic spectra (Fig. 2, main text), thereby confirming that rotation diffusion does not play any role in the polarized kinetics (see main text, §2.4.2). Slightly but significantly poorer fits were obtained with a sum of only 3 exponential components followed by a plateau, especially for W370F. The role of the fourth component is particularly sensitive on the long timescale (hundreds of ps) of the kinetics and, indirectly, to the match this fit provides to the anisotropy data (Fig. S8-B and Fig. S9-B).

Table S4. Time constants of the global mutiexponential fit of the polarized transient absorption spectra of Xl64, WT and W370F. Fit errors (2σ) are indicated in small characters. The average residue of the fit is given as well as the coefficient of determination (R^2).

	τ_1 (ps)	τ_2 (ps)	τ_3 (ps)	τ_4 (ps)	Avg. residue	R^2
WT	0.48 ± 0.01	9.7 ± 0.4	40 ± 1	196 ± 5	4.6×10^{-5}	0.99974
W370F	0.46 ± 0.01	11.7 ± 0.5	50 ± 1	771 ± 29	4.6×10^{-5}	0.99980

The corresponding decay-associated difference spectra (DADS) are shown for reference in Fig. S6 for WT and Fig. S7 for W370F. Panel C of those figures shows the isotropic DADS deduced from the polarized ones.

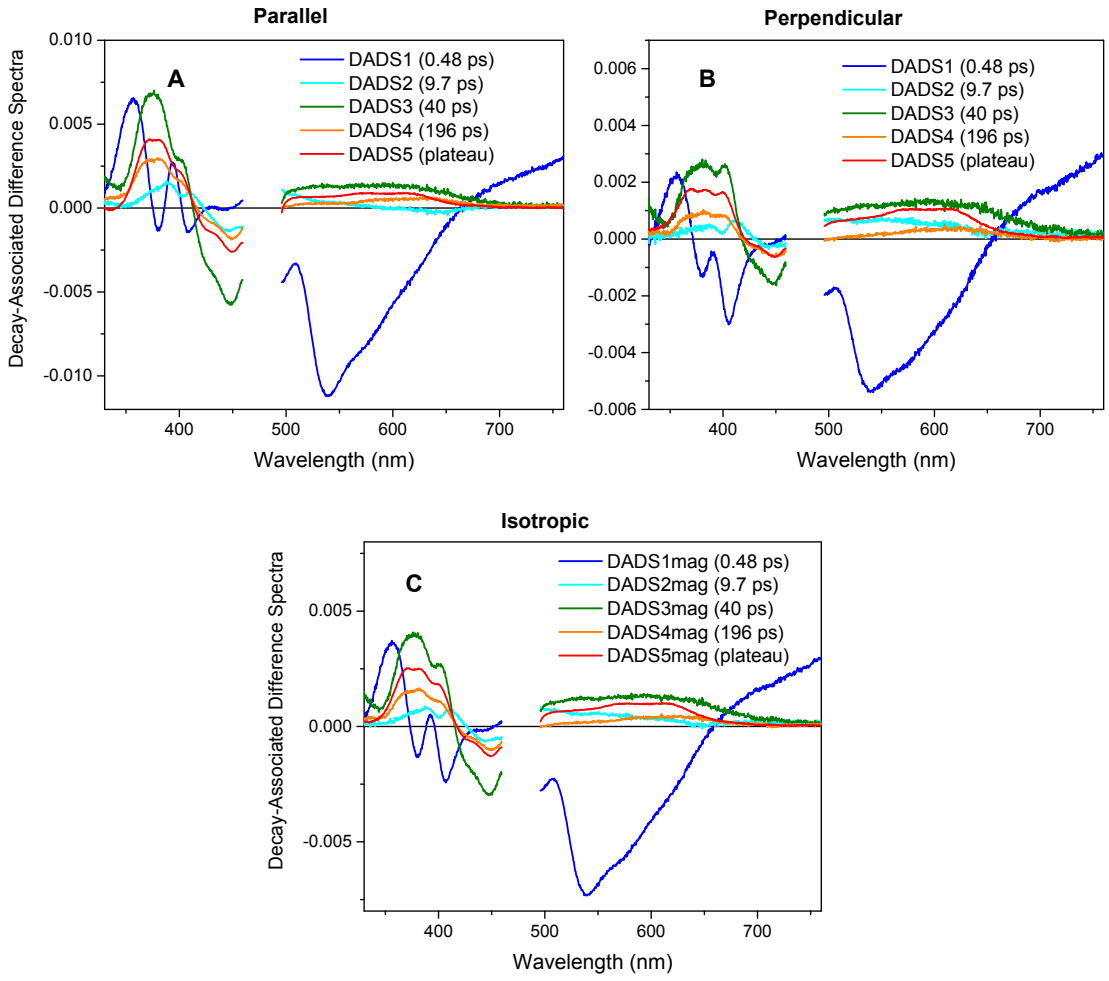

Fig. S6. Polarization-dependent DADS associated to the global analysis of the WT measurement with a sum of 4 exponentials and a plateau. A) Parallel data. B) Perpendicular data. C) Isotropic data.

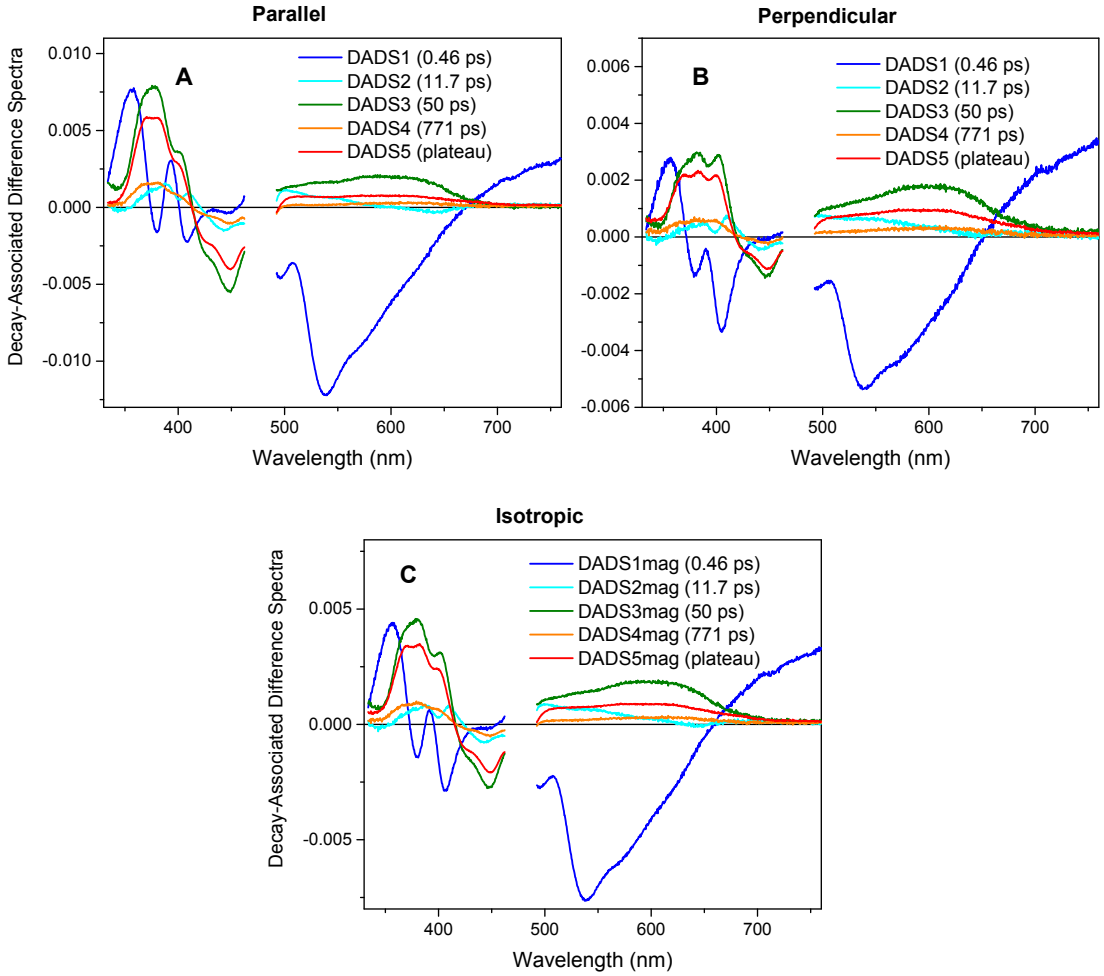

Fig. S7. Polarization-dependent DADS associated to the global analysis of the W370F measurement with a sum of 4 exponentials and a plateau. A) Parallel data. B) Perpendicular data. C) Isotropic data.

The quality of the fits, recast in terms of isotropic transient absorption and anisotropy, is illustrated in Fig. S8 (WT) and Fig. S9 (W370F).

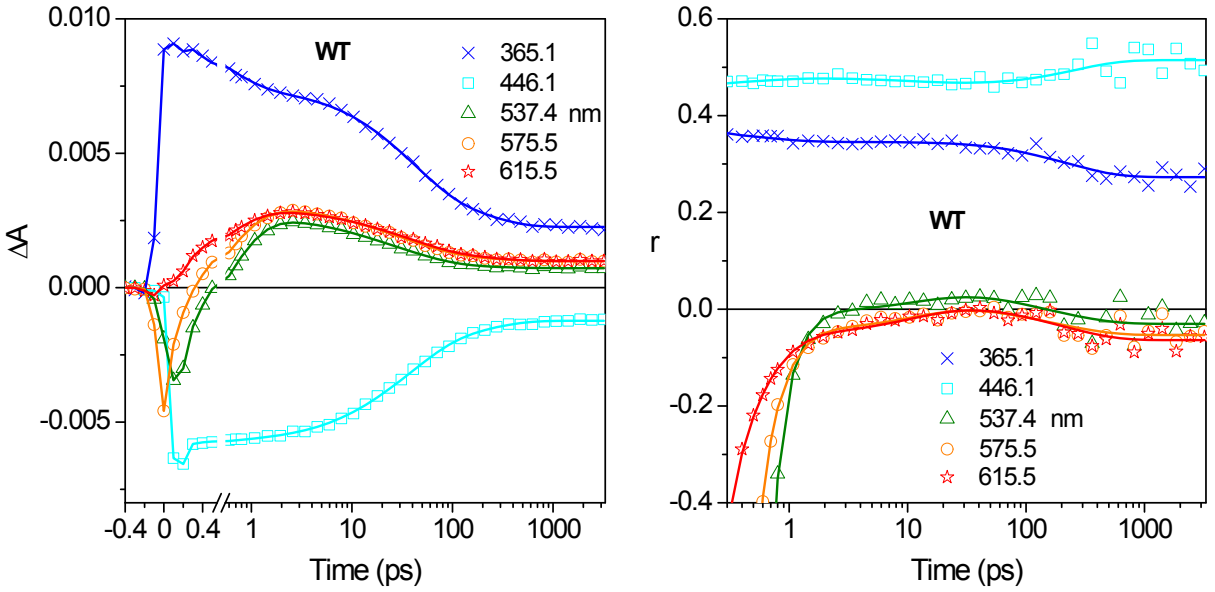

Fig. S8. Kinetic traces of isotropic transient absorption (A) and anisotropy (B) of WT-Xl64, at selected wavelengths. The data have been averaged over about 2 nm (5 pixels). The continuous lines are deduced from the global fit of the polarized transient absorption data.

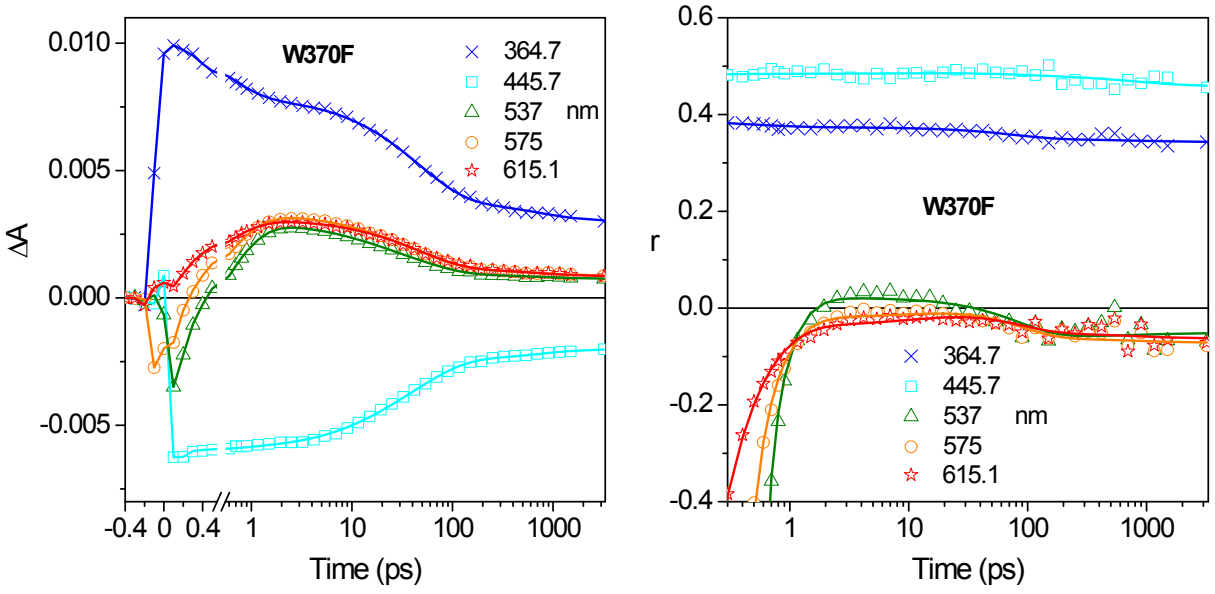

Fig. S9. Kinetic traces of isotropic transient absorption (A) and anisotropy (B) of W370F-Xl64, at selected wavelengths. The data have been averaged over about 2 nm (5 pixels). The continuous lines are deduced from the global fit of the polarized transient absorption data.

Polarized evolution-associated difference spectra (EADS) were calculated as explained in §2.5 of the main text (not shown). From them, isotropic EADS were deduced and are presented in

Fig. 3 of the main text. Anisotropy spectra were derived as well (called evolution-associated anisotropy spectra; EAAS) and are shown for reference in Fig. S10.

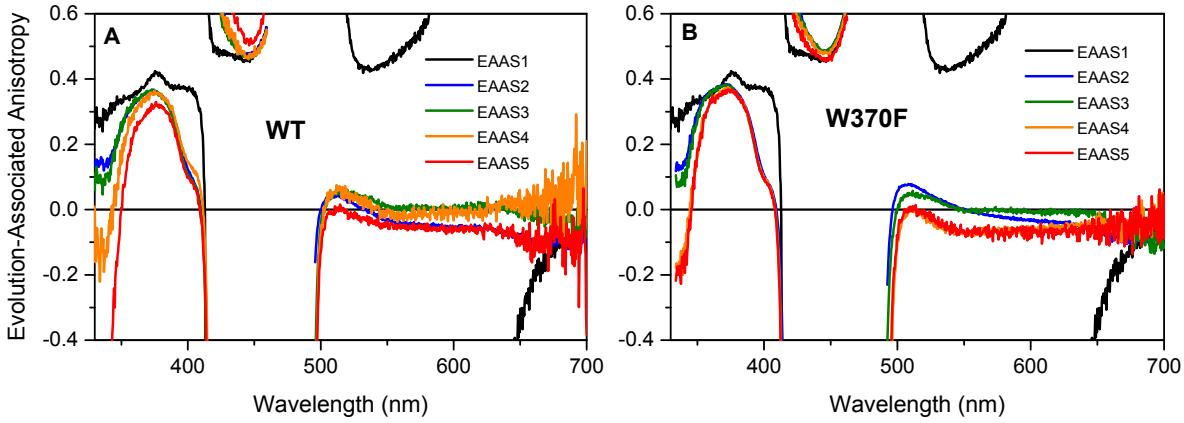

Fig. S10. Evolution-associated anisotropy spectra (EAAS) of WT-Xl64 (A) and its W370F mutant (B).

7. Reference absorption spectra used for the identification of the photoproducts

In order to identify the photoproducts obtained after decay of the excited state (see Section 4.1 of the main text) we compared the EADS 2 to 5 of Xl64 (WT and W370F) to simulated transient absorption spectra corresponding to different combinations of semi-reduced ($FAD^{\bullet-}$ or $FADH^{\bullet}$) and oxidized ($WH^{\bullet+}$ or $W^{\bullet}$ or $YO^{\bullet}$) species. Fig. S11 reports the reference spectra used to construct the simulated spectra. They were taken from the published works of Liu *et al.*[14] ($FAD^{\bullet-}$ in *Anopheles gambiae* cryptochrome 1, noted AgCRY1), Schleicher *et al.*[11] (FAD_{ox} and $FADH^{\bullet}$ in Xl64), Solar *et al.*[15] ($WH^{\bullet+}$, $W^{\bullet}$) and Giese *et al.*[16] ($YO^{\bullet}$). The FAD_{ox} spectrum was scaled to $\varepsilon = 11300\ M^{-1}\ cm^{-1}$ at 448 nm,[17] as described in Müller *et al.*[12] Fig. S12 shows the corresponding simulated differential spectra.

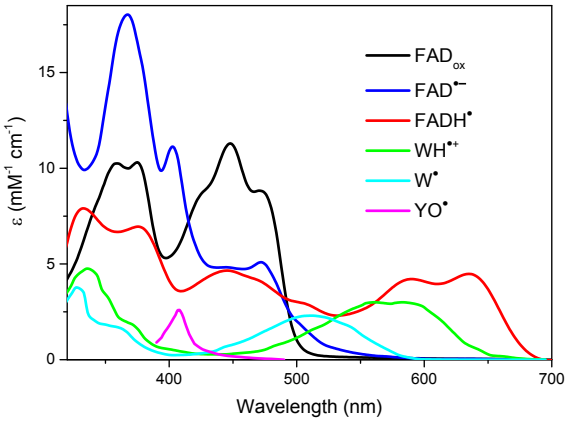

Fig. S11. Reference spectra used to construct the simulated spectra. They are reproduced from the published works of Giese *et al.*[16] (FAD$^{\bullet-}$ in AgCRY1), Schleicher *et al.*[11] (FAD$_{ox}$ and FADH$^{\bullet}$ in Xl64), Solar *et al.*[15] (WH$^{\bullet+}$, W$^{\bullet}$) and Giese *et al.*[16] (YO$^{\bullet}$).

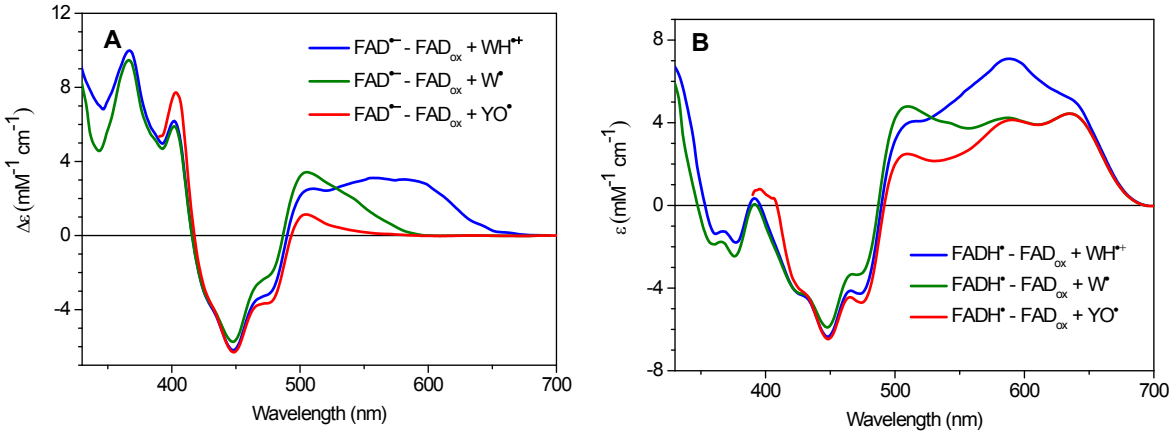

Fig. S12. Simulated differential molar extinction coefficient spectra of putative photoproducts obtained after photoreduction of FAD$_{ox}$. The cases of FAD$_{ox}$ reduction into FAD$^{\bullet-}$ and into FADH$^{\bullet}$ are displayed in panels A and B, respectively. The spectra were built from published spectra shown in Fig. S11.

8. Quantum yield of charge separation

Extending the analysis of the dynamics developed in §4.3 of the main text, it is interesting to try to quantify losses by charge recombination and to estimate the quantum yield attached to each kinetic step. We used for that purpose the evolution of the amplitudes of the absorption changes at wavelengths where they should be dominated by flavin contributions (around 450 and 380 nm; see Fig. S11) and should hence not be much affected by differences in band shape and amplitude

between the different Trp cation radicals that are most evident above 500 nm. Table S5 displays amplitude ratios (a_{ij}) at 448 nm and at 380 nm for different pairs of EADS, both for WT and W370F. EADS1 is not included in this table because its spectral shape is rather different from the other EADS (involvement of FAD_{ox}^* instead of $FAD^{\bullet-}$). The quantum yield of the first ET is however very likely close to 1 because of the extreme rate of the process (~0.5 ps). Published data on oxidized EcCPD[18] indicate a yield of the primary ET of 0.95, while it is in fact slightly slower (0.8 ps) than for Xl64. Factor a_{25} may thus be considered as a rough estimate of the quantum yield of final charge separation. For WT, yields of 0.22 and 0.29 are obtained for estimations at 448 and 380 nm, respectively. The deviation may be due to the uncertain contributions of $W_DH^{\bullet+}$ at these wavelengths. Higher and consistent yields (0.35 and 0.36, respectively) are obtained for W370F. These values may be compared to an estimation by Müller *et al.*[12] using an actinometric approach on the nanosecond scale. They reported a quantum yield of 0.30 ± 0.05 for the final radical pair in W370F and assumed a similar yield for WT because of similar signal amplitudes above 500 nm and in the near UV. A difference in amplitudes appeared, however, around 450 nm and was tentatively attributed to a specific contribution of $W_DH^{\bullet+}$ around 450 nm. A re-evaluation of the yield in WT from the previous data[12] around 450 nm alone, assuming no specific contribution of $W_DH^{\bullet+}$, results in a quantum yield of *ca.* 0.2, similar to the present estimate at 448 nm.

Table S5. Ratios of the bleaching band maxima of different EADS. Factor a_{ij} is defined as the ratio taken between the value of EADSj and that of EADSi. The values were measured at both 448 and 380 nm.

		a_{23}	a_{34}	a_{45}	a_{25}
WT	448 nm	0.77	0.46	0.62	0.22
	380 nm	0.81	0.53	0.68	0.29
W370F	448 nm	0.78	0.55	0.82	0.35
	380 nm	0.82	0.55	0.80	0.36

For the present approach, Table S5 reveals that the main source of difference between WT and W370F is the last kinetic step (represented by a_{45}) which appears to have a larger yield for W370F (0.82 and 0.80, resp.) than for WT (0.62 and 0.68, resp.). Let us recall that the 4th kinetic component is associated to the final localization of the oxidation hole on W_D in WT and to the

stabilization of the $FAD^{\bullet-}/W_CH^{\bullet+}$ pair in W370F (see above). The increase of a_{45} in W370F hypothetically suggests that conformational changes induced by the replacement of W370 by F might help stabilizing the $W_CH^{\bullet+}$ radical (in W370F), reducing the back electron transfer phenomenon, that is, delocalization of the positive charge along the chain and recombination at the W_A site. Such a tentative explanation should naturally be taken with care.

9. Nanosecond anisotropy measurements

Extending the work of Müller *et al.*[12] on WT-Xl64 and its W370F mutant, the transient absorption anisotropy of these two systems was measured on the sub-microsecond time scale, after excitation of the flavin at 475 nm by 5 ns pulses of ~2mJ/cm^2, delivered by a Nd:YAG pumped optical parametric oscillator (Brillant B/Rainbow, Quantel, France). The monitoring light beam and the detection system were as described,[12] except that the electronic bandwidth was limited to 100 MHz. Absorption changes were recorded with monitoring light polarized either parallel or perpendicular to the polarization of the excitation pulse. 8 or 16 signals were averaged for each orientation. Anisotropy kinetics were then calculated according to Eq. 2 in the main text. Fig. S13 represents the anisotropy kinetics recorded at 562 nm, which is dominated by the contribution of the $WH^{\bullet+}$ radical.

The traces could be fitted by a single-exponential decay, as shown in Fig. S13 (thick continuous lines). The fit parameters, initial value r_{init} and decay time τ_{rot}, are shown in Fig. S13 and recalled in Table S6.

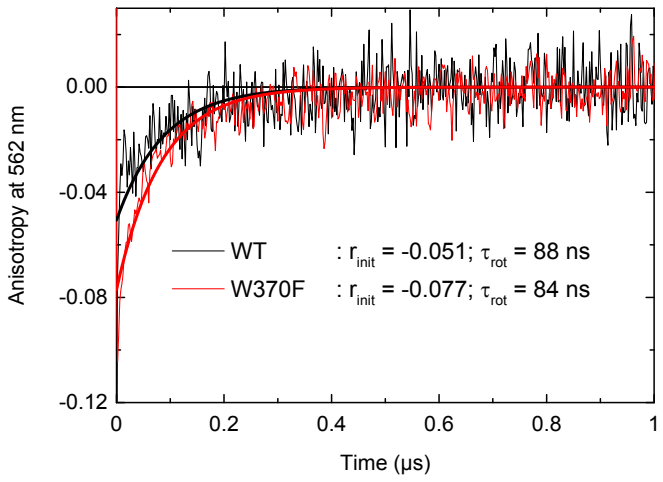

Fig. S13. Transient absorption anisotropy kinetics measured at 562 nm for WT-Xl64 (black) and its W370F mutant (red) after 5-ns excitation at 475 nm. The samples were prepared as described[12] and kept at 8°C during the experiment. They contained ~70 µM photolyase in 50 mM Tris-HCl (pH 8), 50 mM NaCl and 5% (v/v) glycerol. The thick continuous lines represent fits of the data with single-exponential decays. The parameters of the fit (initial value r_{init} and decay time τ_{rot}) are recalled in the figure.

The decay time (~85 ns in both cases) can unambiguously be attributed to the slow rotational diffusion of the protein as a whole. As far as the initial anisotropy (r_{init}) is concerned and according to the findings of Müller *et al.*,[12] the value of WT (-0.051) likely arises from the W_D tryptophan, while that of W370F (-0.077) is assigned to W_C.

Table S6. Fit parameters of the transient absorption anisotropy kinetics measured at 562 nm for WT-Xl64 and its W370F mutant after 5-ns excitation at 475 nm. Fit errors (2σ) are indicated in small characters.

	r_{init}	τ_{rot} (ns)
WT	-0.051 ± 0.006	88 ± 7
W370F	-0.077 ± 0.006	84 ± 5

10. Basic reaction scheme

In order to help following the data analysis and discussion sections of the main text, we provide in Fig. S14 a basic reaction scheme of the photoreduction of FAD_{ox} by the Trp tetrad of WT-Xl64. This very simplified scheme is provided as a mere guideline; it does include potential contributions to the dynamics, discussed in the main text, coming from putatively hot $W_AH^{\bullet+}$ radical, from the alternative $W_{B'}H^{\bullet+}$ radical or from direct electron transfer from W_C to $W_AH^{\bullet+}$ by the suggested flickering resonance mechanism.

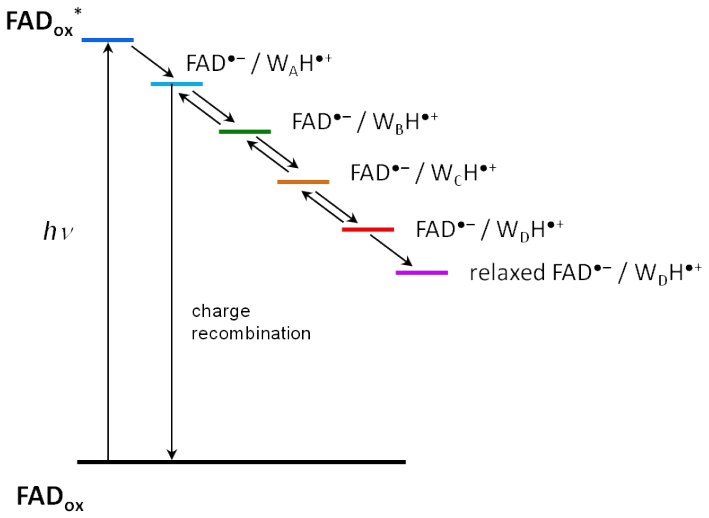

Fig. S14. Basic reaction scheme for the photoreduction of FAD_{ox} by the Trp tetrad of WT-Xl64, used as a guideline for the data analysis and discussion.

Supplementary references

1 M. J. Maul, T. R. M. Barends, A. F. Glas, M. J. Cryle, T. Domratcheva, S. Schneider, I. Schlichting and T. Carell, *Angew. Chem. Int. Ed.*, 2008, **47**, 10076.

2 K. Arnold, L. Bordoli, J. Kopp and T. Schwede, *Bioinformatics*, 2006, **22**, 195; F. Kiefer, K. Arnold, M. Kuenzli, L. Bordoli and T. Schwede, *Nucleic Acids Res.*, 2009, **37**, D387; N. Guex, M. C. Peitsch and T. Schwede, *Electrophoresis*, 2009, **30**, S162; M. Biasini, S. Bienert, A. Waterhouse, K. Arnold, G. Studer, T. Schmidt, F. Kiefer, T. G. Cassarino, M. Bertoni, L. Bordoli and T. Schwede, *Nucleic Acids Res.*, 2014, **42**, W252.

3 B. R. Brooks, C. L. Brooks, A. D. Mackerell, L. Nilsson, R. J. Petrella, B. Roux, Y. Won, G. Archontis, C. Bartels, S. Boresch, A. Caflisch, L. Caves, Q. Cui, A. R. Dinner, M. Feig, S. Fischer, J. Gao, M. Hodoscek, W. Im, K. Kuczera, T. Lazaridis, J. Ma, V. Ovchinnikov, E. Paci, R. W. Pastor, C. B. Post, J. Z. Pu, M. Schaefer, B. Tidor, R. M. Venable, H. L. Woodcock, X. Wu, W. Yang, D. M. York and M. Karplus, *J. Comput. Chem.*, 2009, **30**, 1545.

4 F. Cailliez, P. Muller, T. Firmino, P. Pernot and A. de la Lande, *J. Am. Chem. Soc.*, 2016, **138**, 1904.

5 M. Byrdin, S. Villette, A. Espagne, A. P. M. Eker and K. Brettel, *J. Phys. Chem. B*, 2008, **112**, 6866.

6 B. Valeur and M. N. Berberan-Santos, *Molecular Fluorescence: Principles and Applications, 2nd Edition*, Wiley-VCH, 2013.

7 W. A. Eaton, J. Hofrichter, M. W. Makinen, R. D. Andersen and M. L. Ludwig, *Biochemistry*, 1975, **14**, 2146.

8 T. Climent, R. Gonzalez-Luque, M. Merchan and L. Serrano-Andres, *J. Phys. Chem. A*, 2006, **110**, 13584.

9 A. Crespo, A. G. Turjanski and D. A. Estrin, *Chem. Phys. Lett.*, 2002, **365**, 15.
10 J. D. Chai and M. Head-Gordon, *Phys. Chem. Chem. Phys.*, 2008, **10**, 6615.
11 E. Schleicher, K. Hitomi, C. W. M. Kay, E. D. Getzoff, T. Todo and S. Weber, *J. Biol. Chem.*, 2007, **282**, 4738.
12 P. Müller, J. Yamamoto, R. Martin, S. Iwai and K. Brettel, *Chem. Commun.*, 2015, **51**, 15502.
13 J. Yamamoto, R. Martin, S. Iwai, P. Plaza and K. Brettel, *Angew. Chem. Int. Ed.*, 2013, **52**, 7432.
14 B. Liu, H. Liu, D. Zhong and C. Lin, *Curr. Opin. Plant Biol.*, 2010, **13**, 578.
15 S. Solar, N. Getoff, P. S. Surdhar, D. A. Armstrong and A. Singh, *J. Phys. Chem.*, 1991, **95**, 3639.
16 B. Giese, M. Wang, J. Gao, M. Stoltz, P. Müller and M. Graber, *J. Org. Chem.*, 2009, **74**, 3621.
17 P. Macheroux, in *Flavoprotein Protocols*, eds. S. K. Chapman and G. A. Reid, 1999, pp. 1.
18 Z. Y. Liu, C. Tan, X. M. Guo, J. Li, L. J. Wang, A. Sancar and D. P. Zhong, *Proc. Natl. Acad. Sci. USA*, 2013, **110**, 12966.